Substituent Effects on Electrochemical and Electrochromic Properties of Aromatic Polyimides with 4-(Carbazol-9-yl)triphenylamine Moieties

Hui-Min Wang, Sheng-Huei Hsiao

Department of Chemical Engineering and Biotechnology, National Taipei University of Technology, Taipei 10608, Taiwan
Correspondence to: S.-H. Hsiao (E-mail: shhsiao@ntut.edu.tw)

Received 19 December 2013; accepted 7 January 2014; published online 7 February 2014
DOI: 10.1002/pola.27103

ABSTRACT: Three series of aromatic polyimides with 4-(carbazol-9-yl)triphenylamine moieties were prepared from the polycondensation reactions of 4,4′-diamino-4"-(carbazol-9-yl) triphenylamine (1), 4,4′-diamino-4"-(3,6-di-*tert*-butylcarbazol-9-yl)triphenylamine (*t*-Bu-1), and 4,4′-diamino-4"-(3,6-dimethoxycarbazol-9-yl)triphenylamine (MeO-1), respectively, with various commercially available tetracarboxylic dianhydrides. In addition to high thermal stability and good film-forming ability, the resulting polyimides exhibited an ambipolar electrochromic behavior. The polyimides based on *t*-Bu-1 and MeO-1 revealed higher redox-stability and enhanced electrochromic performance than the corresponding ones based on 1 because the active sites of their carbazole units are blocked with bulky *t*-butyl or electron-donating methoxy groups. © 2014 Wiley Periodicals, Inc. J. Polym. Sci., Part A: Polym. Chem. **2014**, *52*, 1172–1184

KEYWORDS: carbazole; electrochemistry; electrochromic polymers; polyimides; redox polymers; triphenylamine

INTRODUCTION Aromatic polyimides are characterized as highly thermally stable polymers with a favorable balance of physical and chemical properties. They are commercially important materials used extensively as dielectric films and coatings in a wide range of high technology applications.[1] However, rigidity of the backbone and strong interchain interactions result in high melting or glass-transition temperatures (T_g) and limited solubility in most organic solvents. Thus, polyimide processing is generally carried out via poly(amic acid) precursor and then converted to polyimide by vigorous thermal or chemical cyclodehydration. This process has inherent problems such as emission of volatile byproducts and storage instability of poly(amic acid) solution. To overcome these problems, many attempts have been made to the synthesis of soluble and processable polyimides in fully imidized form while maintaining their excellent properties.[2] The majority of methods used for improving the solubility while maintaining the high-temperature performance of polyimides have involved the structural modifications of dianhydride and diamine monomers. Typical approaches include the introduction of flexible linkages, kinked or unsymmetrical structures, bulky packing-disruptive units, and bulky lateral groups into the polymer backbone.[3]

Triarylamine[4] and carbazole[5] derivatives are well known as their photo and electroactive properties that find optoelectronic applications as photoconductors, hole-transporters, light-emitters, and memory devices. Polymers bearing triarylamine units are receiving considerable interest as ideal hole-transporting materials in various optoelectronic device applications such as organic light-emitting diodes because of the strong electron-donating and hole-transporting/injecting properties of triarylamine units.[6] Additionally, triarylamines can be easily oxidized to form stable radical cations, and the oxidation process is always associated with a strong change of coloration. Thus, many triarylamine-based polymers have been investigated for electrochromic applications.[7] Since 2005, Liou's and our groups have developed several high-performance polymer systems such as aromatic polyimides[8] and polyamides[9] with the triarylamine unit for potential electrochromic applications. Our strategy was to synthesize the triarylamine-containing monomers such as diamines and dicarboxylic acids that were then reacted with the corresponding comonomers via conventional polycondensation techniques. The obtained polymers possessed a well-defined structure, high thermal stability, and good mechanical properties. Most of them exhibited good solubility in many organic solvents due to the incorporation of packing-disruptive, three-dimensional triarylamine unit along the polymer backbone. They could form uniform, transparent amorphous thin films by simple solution processing, which is advantageous for their ready fabrication of large-area, thin-film devices.

Previous studies have demonstrated that aromatic polyamides and polyimides containing 4-(carbazol-9-yl)triphenylamine (CzTPA) segments show attractive electrochemical and

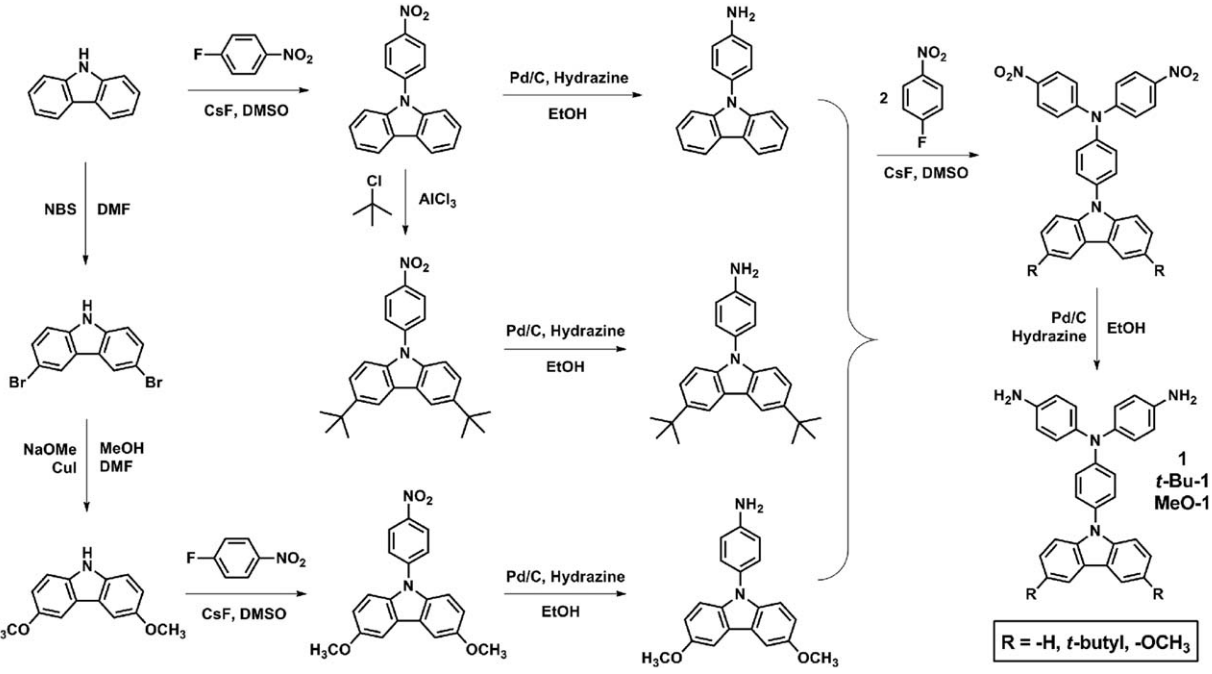

SCHEME 1 Synthetic routes to diamine monomers **1**, ***t*-Bu-1** and **MeO-1**.

electrochromic properties.[10] These polymers reveal good redox stability during the first oxidation process at a lower applied potential, and the oxidation process is accompanied with a noticeable change of absorption in the visible and near-infrared regions. However, the second oxidation process of these polymers at a higher applied potential is not reversible, possibly because of the electrochemical coupling of carbazoles through the active C-3 and C-6 sites.[11] This may result in undesired decreased device performance, localized color defects, and heterogeneous color contrast of this kind of electrochromic materials. It has been reported[12] that the incorporation of bulky groups such as *tert*-butyl or triphenylsilyl group on the electrochemically active sites (C-3 and C-6) of carbazole leads to enhanced electrochemical and morphological stability of the carbazole derivatives. As reported in our recent publications,[13,14] redox-stable aromatic polyamides and polyimides with valuable electrochromic properties have been prepared by using 4,4′-diamino-4″-(3,6-di-*tert*-butylcarbazol-9-yl)triphenylamine (***t*-Bu-1**) as the diamine component. Very recently, we have also reported the synthesis and characterization of 4,4′-diamino-4″-(3,6-dimethoxycarbazol-9-yl)triphenylamine (**MeO-1**) and its derived polyamides.[15] The polyamides showed an enhanced electrochemical and electrochromic stability due to the substitution of active sites of the carbazole unit with electron-donating methoxy groups. Turning our attention to enhancing electrochemical and electrochromic stability of the CzTPA-based polyimides, we have synthesized a series of aromatic polyimides from the polymerization reactions of diamine **MeO-1** with aromatic dianhydrides. The electrochemical and electrochromic properties of these polyimides were compared with those of structurally similar polyimides derived from ***t*-Bu-1** and 4,4′-diamino-4″-(carbazol-9-yl)triphenylamine (**1**). The effects of incorporating methoxy or *tert*-butyl groups on the C-3 and C-6 positions of pendent carbazole units on the properties of these polyimides were investigated.

EXPERIMENTAL

Materials

4,4′-Diamino-4″-(carbazol-9-yl)triphenylamine (**1**) (mp = 192–195 °C),[10(a)] 4,4′-diamino-4″-(3,6-di-*tert*-butylcarbazol-9-yl)triphenylamine (***t*-Bu-1**) (mp = 273–274 °C),[13] and 4,4′-diamino-4″-(3,6-dimethoxycarbazol-9-yl)triphenylamine (**MeO-1**) (mp = 131–132 °C)[15] were synthesized according to the previously reported procedures. Their synthetic routes are shown in Scheme 1. Details of the synthesis and characterization data of these CzTPA-based diamine monomers have been described in our previous publications.[10(a),13,15] According to a literature procedure,[16] the model compounds, 9-phenylcarbazole (**M1**), 3,6-di-*tert*-butyl-9-phenylcarbazole (**M2**), and 3,6-dimethoxy-9-phenylcarbazole (**M3**), were synthesized via Ullmann C—N coupling reaction of iodobenzene with carbazole, 3,6-di-*tert*-butyl-9H-carbazole and 3,6-dimethoxy-9H-carbazole, respectively, by using copper powder and K_2CO_3 in tri(ethylene glycol) dimethyl ether (TEGDME). *N,N*-Dimethylacetamide (DMAc) was dried over calcium hydride for 24 h, distilled under reduced pressure, and stored over 4 Å molecular sieves in a sealed bottle. Commercially available tetracarboxylic dianhydrides such as pyromellitic dianhydride (PMDA; **2a**; Aldrich) was purified by recrystallization from acetic anhydride. The other dianhydrides that included 3,4,3′,4′-biphenyltetracarboxylic dianhydride (BPDA; **2b**; Oxychem), 4,4′-oxydiphthalic dianhydride (ODPA; **2c**; Oxychem), and 2,2-bis(3,4-dicarboxyphenyl)hexafluoropropane dianhydride (6FDA; **2d**; Hoechst Celanese)

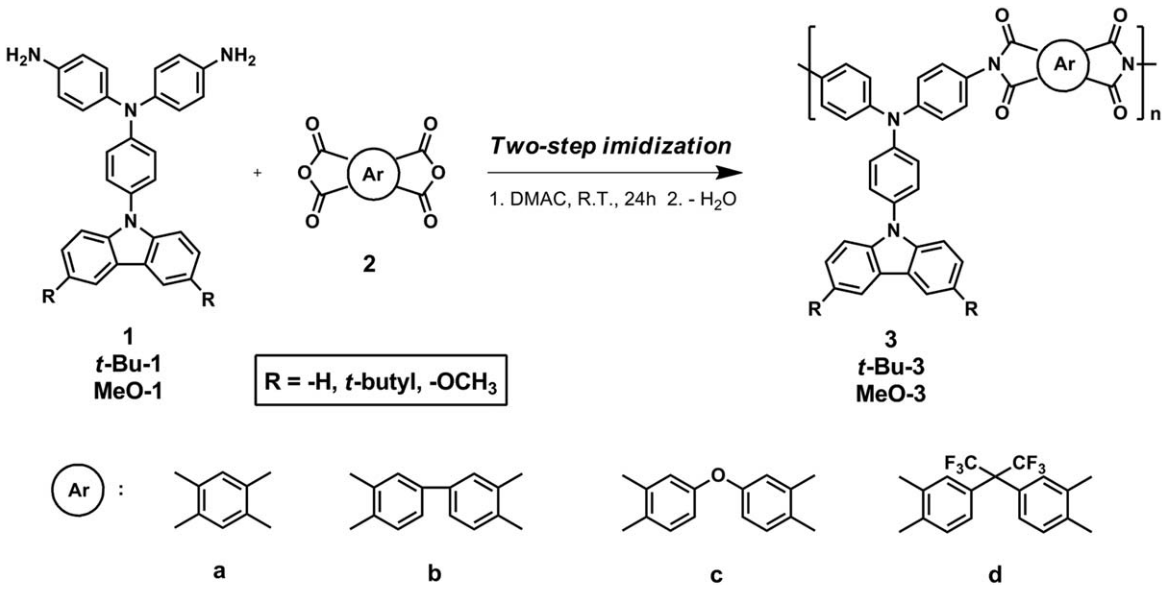

SCHEME 2 Synthesis of polyimides.

were heated at 250 °C *in vacuo* for 3 h before use. Tetra-*n*-butylammonium perchlorate (Bu_4NClO_4, TCI) was recrystallized twice from ethyl acetate and then dried *in vacuo* before use. All other reagents were used as received from commercial sources.

Polymer Synthesis

A typical example of the synthesis of polyimide **MeO-3d** is described as follows: The diamine monomer **MeO-1** (0.530 g, 1.06 mmol) was dissolved in 9.5 mL of dried DMAc in a 50-mL round-bottom flask. Then 6FDA (0.470 g, 1.06 mmol) was added into the diamine solution in one portion. Thus, the solid content of the solution is ~10 wt %. The mixture was stirred at room temperature for about 24 h to yield a highly viscous poly(amic acid) solution. The inherent viscosity of the resulting poly(amic acid) was 1.80 dL g^{-1}, measured in DMAc at a concentration of 0.5 g dL^{-1} at 30 °C. For the thermal imidization process, about 5 g of the obtained poly(amic acid) solution was transferred to a 7-cm glass Petri dish, which was placed overnight in a 90 °C oven for the slow release of the casting solvent. The poly(amic acid) in the form of solid film was converted to polyimide **MeO-3d** by successive heating under vacuum at 150 °C for 30 min, 200 °C for 30 min, 250 °C for 30 min, and 300 °C for 1 h. For the chemical imidization method, 2 mL of acetic anhydride and 1 mL of pyridine were added to the remaining poly(amic acid) solution, and the mixture was heated at 100 °C for 1 h to effect a complete imidization. The homogenous polymer solution was poured slowly into 200 mL of stirring methanol giving rise to a reddish brown precipitate that was collected by filtration, washed thoroughly with hot water and methanol, and dried. A polymer solution was made by the dissolution of about 0.5 g of the polyimide sample in 10 mL of hot DMAc. The homogeneous solution was poured into a 9-cm glass Petri dish, which was placed in a 90 °C oven overnight for the slow release of the solvent, and then the film was stripped off from the glass substrate and further dried in vacuum at 160 °C for 6 h. The IR spectrum of **MeO-3d** (film) exhibited characteristic imide absorption bands at 1783 (asymetrical C=O stretch) and 1732 cm^{-1} (symmetrical C=O stretch). ^1H NMR (500 MHz, $CDCl_3$, δ, ppm) [for the peak assignments, see Fig. 2(c)]: 3.94 (s, 6H, —OCH_3), 7.05 (d, $J = 7.0$ Hz, 2H, H_c), 7.36–7.39 (m, 12H, $H_d + H_f + H_g + H_h$), 7.49 (d, $J = 8.0$ Hz, 2H, H_e), 7.55 (s, 2H, H_a), 7.87 (d, $J = 7.5$ Hz, 2H, H_j), 7.97 (s, 2H, H_k), 8.05 (d, $J = 8.0$ Hz, 2H, H_i).

Measurements

Infrared spectra were recorded on a Horiba FT-720 FT-IR spectrometer, and the ^1H and ^{13}C NMR spectra on a 500 MHz instrument (Bruker AVANCE-500 FT-NMR system) using DMSO-d_6 as the solvent and tetramethylsilane as the internal standard. Elemental analyses were run in a Heraeus VarioEL-III CHNS elemental analyzer. The inherent viscosities of the polymers were determined at 0.5 g/dL concentration using an Ubbelohde viscometer at 30 °C. Thermogravimetric analyses (TGA) were conducted with a TA instruments Q50 TGA, at a heating rate of 20 °C min^{-1} in flowing nitrogen or air (flow rate = 20 cm^3 min^{-1}). DSC analyses were performed on a PerkinElmer DSC4000 differential scanning calorimeter (DSC) at a scan rate of 20 °C min^{-1} under nitrogen. Ultraviolet-visible (UV–vis) spectra of the polymer films were recorded on an Agilent 8453 UV–visible spectrometer. Electrochemistry was performed with a CH Instruments 750A electrochemical analyzer. Voltammograms are presented with the positive potential pointing to the left and with increasing anodic currents pointing downwards. Cyclic voltammetry (CV) was conducted with the use of a three-electrode cell in which ITO (polymer films area about 1 cm^2, 0.8 × 1.25 cm^2) was used as a working electrode. A platinum wire was used as an auxiliary electrode. All cell potentials were taken by using an ALS RE-1B (Ag/AgCl, 3M NaCl) reference electrode.

TABLE 1 Inherent Viscosity and Solubility Behavior of the Chemically Imidized Polyimides

		Solubility[b] in Various Solvents[c]					
Polymer Code	η_{inh}[a] (dL g^{-1})	NMP	DMAc	DMF	DMSO	*m*-Cresol	THF
3a	1.93	+−	+−	+−	+−	−	−
3b	1.74	+−	−	−	−	+h	−
3c	1.69	+h	+h	+h	+h	+h	−
3d	1.50	++	++	++	+h	+h	++
***t*-Bu-3a**	1.36	+−	+−	+−	+−	+−	+−
***t*-Bu-3b**	1.72	+h	−	−	−	+h	−
t-Bu-3c	1.63	++	++	++	+	++	++
t-Bu-3d	2.64	++	++	++	+	++	++
MeO-3a	1.52	+−	+−	+−	+−	+−	+−
MeO-3b	1.46	+h	+−	+−	+−	+h	+−
MeO-3c	0.91	++	+−	+−	+−	+h	+−
MeO-3d	1.80	++	++	++	+	++	++

[a] Inherent viscosity of the poly(amic acid) precursors measured at a concentration of 0.5 dL g^{-1} in DMAc at 30 °C.

[b] Qualitative solubility was tested with 10 mg of a sample in 1 mL of a stirred solvent. ++: soluble at room temperature; +h: soluble on heating; +−: partial soluble on heating; −: insoluble even on heating.

[c] NMP: *N*-methyl-2-pyrrolidone; DMAc: *N,N*-dimethylacetamide; DMF: *N,N*-dimethylformamide; DMSO: dimethyl sulfoxide; THF: tetrahydrofuran.

Ferrocene was used as an external reference for calibration (+0.44 V vs. Ag/AgCl). Spectroelectrochemical experiments were carried out in a cell built from a 1 cm commercial UV-visible cuvette using an Agilent 8453 UV–Visible diode array spectrophotometer. The ITO-coated glass slide was used as the working electrode, a platinum wire as the counter electrode, and a Ag/AgCl cell as the reference electrode. Colorimetric measurements were obtained using a Minolta CS-100A Chroma Meter and the results are expressed in terms of lightness (L^*) and color coordinates (a^*, b^*).

RESULTS AND DISCUSSION

Polymer Synthesis

Three series of aromatic polyimides (**3a–d**, ***t*-Bu-3a-d**, and **MeO-3a-d**) with CzTPA units were prepared in conventional two-step method by the reactions of equal molar amounts of diamine **1**, ***t*-Bu-1**, and **MeO-1**, respectively, with various aromatic dianhydrides (**2a-2d**) to form poly(amic acid)s, followed by the thermal or chemical cyclodehydration (Scheme 2). As shown in Table 1, the poly(amic acid) precursors had inherent viscosities in the range of 0.91-2.64 dL g^{-1}. The molecular weights of these poly(amic acid)s were sufficiently high to permit the casting of flexible and tough poly(amic acid) films, which were subsequently converted into tough polyimide films by stage-by-stage heating to elevated temperatures. For the organosoluble polyimides such as **3d**, ***t*-Bu-3c**, ***t*-Bu-3d**, and **MeO-3d,** flexible and strong films could also be cast directly from their DMAc solutions. The transformation from poly(amic acid) to a polyimide could also be carried out via chemical cyclodehydration by using acetic anhydride and pyridine. Structural features of these polyimides were characterized by IR and NMR analysis. Typical IR spectra of polyimides **3d**, ***t*-Bu-3d**, and **MeO-3d** are illustrated in Figure 1. All polyimides exhibited characteristic imide group absorptions around 1783 and 1732 cm^{-1} (typical of imide carbonyl asymmetrical and symmetrical stretch), 1380 cm^{-1} (C—N stretch), and 1100

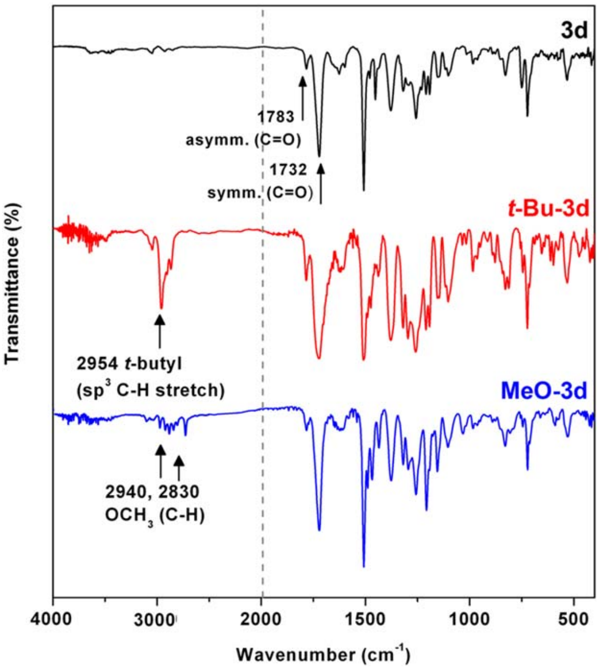

FIGURE 1 IR spectra of polyimides **3d**, ***t*-Bu-3d**, and **MeO-3d**. [Color figure can be viewed in the online issue, which is available at wileyonlinelibrary.com.]

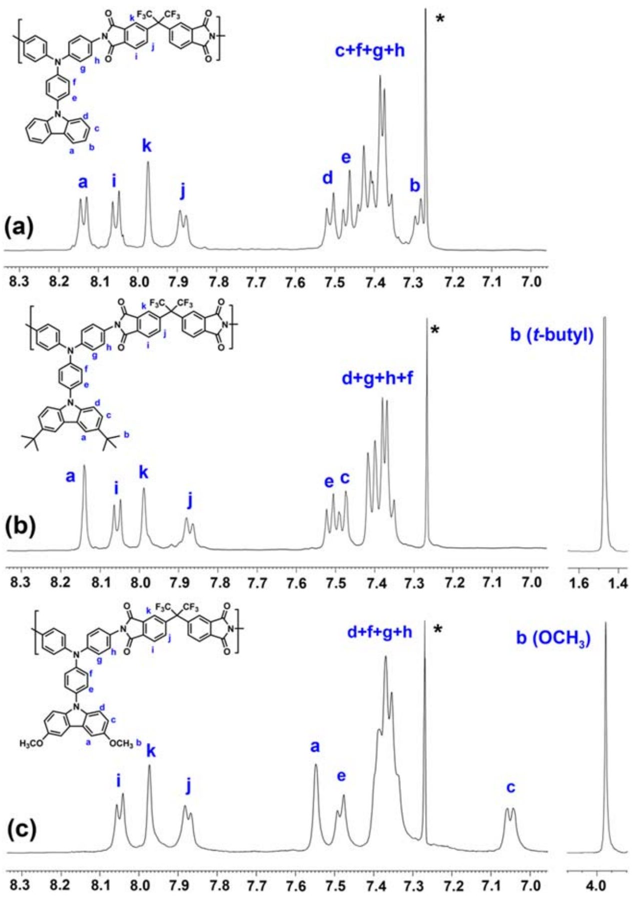

FIGURE 2 ^{1}H NMR spectra of polyimides (a) **3d**, (b) ***t*-Bu-3d**, and (c) **MeO-3d** in $CDCl_3$ (* the solvent peak). [Color figure can be viewed in the online issue, which is available at wileyonlinelibrary.com.]

and 720 cm^{-1} (imide ring deformation). Representative ^{1}H NMR spectra of polyimides **3d**, ***t*-Bu-3d**, and **MeO-3d** in DMSO-d_6 are illustrated in Figure 2, and the resonance peaks are well assigned to the repeating structure of the polymer backbone. All the aromatic protons in the CzTPA moiety resonated in the region of δ 7.05–7.58 ppm, and the protons in the 6FDA component appeared at a lower field of 7.87–8.05 ppm. No resonance peak appeared around 10 ppm in the ^{1}H NMR spectrum support the completed imidization. Assignments of each proton were assisted by the two dimensional H-H COSY NMR spectra shown in Figure 3 and agree well with the structure of the repeating unit. As can be seen from the NMR spectrum shown in Figure 2(c), the electron-donating methoxy group makes the carbazole protons Ha and Hc of **MeO-3d** move significantly to the high fields.

Solubility

The solubility properties of the polyimide samples prepared via the chemical imidization are also listed in Table 1. The polyimides (**3d**, ***t*-Bu-3d**, and **MeO-3d)** derived from 6FDA (**2d)** showed higher solubility than the other ones in the same series because of the additional contribution of the hexafluoroisopropylidene ($-C(CF_3)_2-$) fragment in the polymer backbone which interferes the intermolecular interactions and close packing. They are soluble not only in polar aprotic organic solvents, such as NMP, DMAc, DMF, and DMSO, but also in less polar solvents like THF. For comparison, the **MeO-3** or ***t*-Bu-3** series polyimides showed a slightly enhanced solubility compared to the corresponding **3** ones without the methoxy or *tert*-butyl substituent. This may be a result of increased free volume and decreased interchain interactions caused by the methoxy or *tert*-butyl substitution. Therefore, the good solubility makes these polyimides potential candidates for practical applications in spin-coating and inkjet-printing techniques to afford high performance thin films for optoelectronic devices.

Thermal Properties

The thermal stability and phase transition temperatures of these polyimides were recorded by TGA and DSC. The thermal behavior data of the polyimide are summarized in Table 2. Typical TGA curves of polyimides **3d**, ***t*-Bu-3d**, and **MeO-3d** are depicted in Figure 4. All the prepared polyimides exhibited good thermal stability with insignificant weight loss up to 400 °C under nitrogen or air atmosphere. The 10% weight loss temperatures of these polymers in nitrogen and air were recorded in the range of 529–652 and 492–634

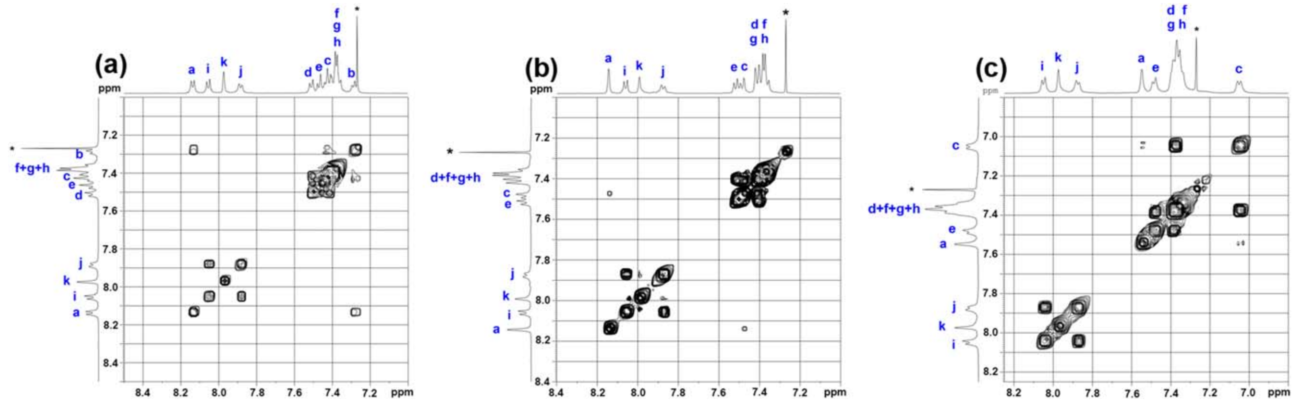

FIGURE 3 H-H COSY NMR spectra of polyimides (a) **3d**, (b) ***t*-Bu-3d**, and (c) **MeO-3d** in $CDCl_3$ (* the solvent peak). [Color figure can be viewed in the online issue, which is available at wileyonlinelibrary.com.]

TABLE 2 Thermal Properties of Polyimides[a]

Polymer code	T_g (°C)[b]	T_d at 10 wt % Loss (°C)[c] In N_2	T_d at 10 wt % Loss (°C)[c] In air	Char yield (%)[d]
3a	–[e]	640	627	72
3b	325	652	634	74
3c	303	648	627	73
3d	310	642	576	72
***t*-Bu-3a**	–[e]	568	552	66
***t*-Bu-3b**	336	583	583	70
***t*-Bu-3c**	320	581	560	66
***t*-Bu-3d**	333	564	565	63
MeO-3a	320	552	498	68
MeO-3b	335	577	525	71
MeO-3c	306	571	514	62
MeO-3d	324	529	492	59

[a] The polymer film sample were heated at 300 °C for 1 h prior to all the thermal analyses.

[b] The sample were heated from 50 to 400 °C at a scan rate of 20 °C/min followed by rapid cooling to 50 °C at −200 °C min^{-1} in nitrogen. The midpoint temperature of baseline shift on the subsequent DSC trace (from 50 to 400 °C at heating rate 20 °C min^{-1}) was defined as T_g.

[c] Decomposition temperature at which a 10% weight loss was recorded by TGA at a heating rate of 20 °C min^{-1}.

[d] Residual weight percentages at 800 °C under nitrogen flow.

[e] No discernible transition was detectable by DSC.

°C, respectively. The amount of carbonized residue (char yield) of these polymers in nitrogen atmosphere was more than 59% at 800 °C. The high char yields of these polymers can be ascribed to their high aromatic content. As expected, the incorporation of methoxy or *tert*-butyl groups into the polymer backbones leads to a slight decrease in thermal stability. Except for **3a** and ***t*-Bu-3a**, other polyimides showed discernible glass-transition temperatures (T_g) of 305–336 °C by DSC. The ***t*-Bu-3** series showed the highest T_g values (320–336 °C) because of the decreased conformational flexibility caused by the bulky *tert*-butyl substituents.

Electrochemical Properties

The electrochemical behavior of model compounds **M1-M3** and the polyimides were investigated by CV. The model compounds were measured in anhydrous acetonitrile (CH_3CN) solution ($\sim 1 \times 10^{-3}$ M) containing 0.1 M Bu_4NClO_4 as the electrolyte, and the polymers were measured by using the solution-cast films on an indium tin oxide (ITO)-coated glass substrate as working electrode which were immersed in a 0.1 M Bu_4NClO_4/acetonitrile solution. The repetitive CV diagrams for model compounds **M1-M3** and representative polyimides **3d**, ***t*-Bu-3d**, and **MeO-3d** are illustrated in Figure 5 for comparison. There are one reversible oxidation redox couples at half-wave potential ($E_{1/2}$) value of +1.08 V ($E_{\text{onset}} = +0.93$ V) and one irreversible oxidation redox wave at $E_{1/2} = +1.40$ V for polyimide **3d** in the first oxidation CV scan [Fig. 5(a)]. In the first reverse negative potential scan, three cathodic peaks were detected. In the second positive potential scan, a new oxidation shoulder appeared in the range of +0.90–1.10 V that was the complementary anodic process of the cathodic peak at a lower potential. The observation of the new redox couple in the second potential scan implies that the carbazole radical cations were involved in very fast electrochemical reactions that produced a new structure that was easier to oxidize than was the parent carbazole. This can be further evidenced by the CV of model compound **M1**. As shown in Figure 5(d), in the first oxidation scan, a sharp peak at $E_{\text{p,a}} = +1.50$ V is observed. In the reverse scan, two reduction waves at $E_{\text{p,c}} = +1.21$ and +0.99 V are observed, respectively. In the continuous scans, an oxidation wave at $E_{\text{p,a}} = +1.10$ V gradually grows, indicative of a new species formation. As reported by Ambrose and co-workers in their pioneering work[11] devoted to anodic oxidation of carbazole and various *N*-substituted carbazoles, ring-ring coupling is the predominant pathway, the carbazole radical cation yielding 3,3′ (6)-bicarbazyls. Similar results have also been reported in recent publications.[13–15] In contrast, model compounds **M2** and **M3** exhibit a reversible redox wave at $E_{1/2} = +1.23$ and +1.01 V, respectively, and continuous cycling does not generate any new wave in 0.0 ~ +1.50 V region [Figure 5(e,f)]. Therefore, it is possible to prevent the irreversible coupling reactions by incorporating bulky *tert*-butyl or electron-donating methoxy substituents at the electrochemically active C-3 and C-6 sites on the carbazole unit of the CzTPA segment. As shown in Figure 5(b,c), polyimide ***t*-Bu-3d** shows two reversible oxidation redox couples at the $E_{1/2} = +1.05$ V ($E_{\text{onset}} = +0.88$ V) and +1.28 V, and **MeO-3d** shows two reversible oxidation redox couples at the $E_{1/2} = +0.90$ V ($E_{\text{onset}} = +0.78$ V) and +1.19 V. The shift to lower oxidation potentials for polyimide **MeO-3d** is conceivably due to the electron-donating effect of the methoxy groups. The other polyimides show a similar CV behavior and their oxidation potentials are compiled in Table 3. As illustrated in Figure 6, model compounds **M1**, **M2**, and **M3** revealed oxidation peaks at $E_{\text{p.a}} = 1.50$, 1.40,

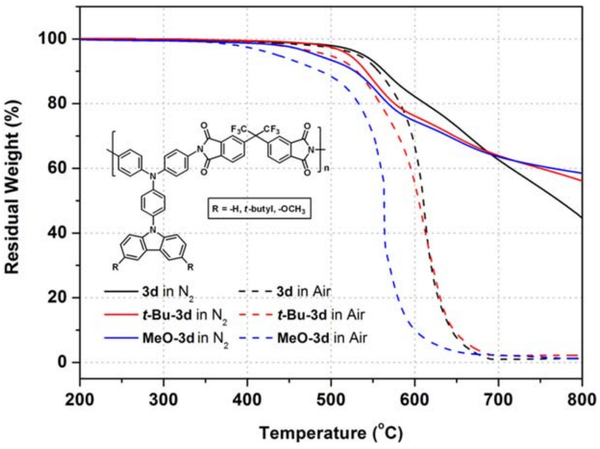

FIGURE 4 TGA thermograms of polyimides **3d**, ***t*-Bu-3d**, and **MeO-3d** in both air and nitrogen atmospheres at a scan rate of 20 °C min^{-1}. [Color figure can be viewed in the online issue, which is available at wileyonlinelibrary.com.]

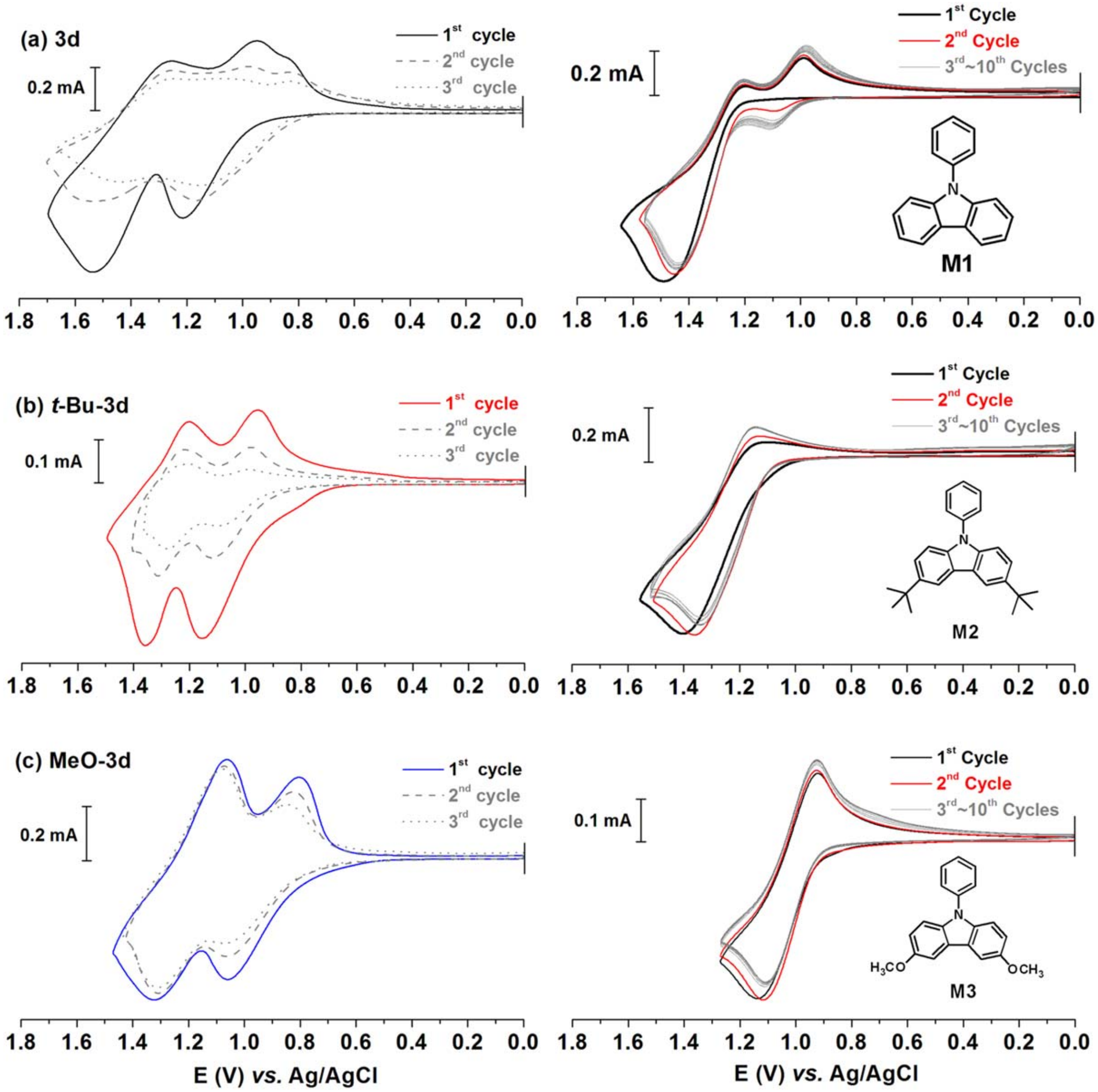

FIGURE 5 Repeated anodic CV diagrams of the cast films of polyimides (a) **3d**, (b) ***t*-Bu-3d**, and (c) **MeO-3d** on the ITO-coated glass substrate and the solutions ($\sim 1 \times 10^{-3}$ M) of model compounds (d) **M1**, (e) **M2**, and (f) **M3** in 0.1 M Bu_4NClO_4/CH_3CN at a scan rate of 50 mV/s. [Color figure can be viewed in the online issue, which is available at wileyonlinelibrary.com.]

and 1.12 V, respectively. Based on the oxidation potentials of these model compounds, we propose the possible oxidative order of the redox centers for polyimides **3d**, ***t*-Bu-3d** and **MeO-3d** (see Fig. 6). It is interesting to note that the *N*-phenylcarbazole unit might oxidize earlier than the triphenylamine core in polyimide **MeO-3d** because of the electron-donating methoxy substituents.

These polyimides also show one or two quasi-reversible waves in the negative side because of the reduction of imide segments. Typical cathodic CV diagrams of polyimides **MeO-3** series are depicted in Figure 7. Redox reactions for the diimide systems shown in the bottom of Figure 7 represent a possible distribution of electron density for the reduced forms, which can also be described by other resonance forms due to the charge delocalization. Reduction of the imide groups may induce increased quinoid character due to charge separation by the ring structure to minimize the electron–electron repulsion. The CV curve of PMDA polyimide **MeO-3a** [Fig. 7(a)] shows that the pyromellitimide groups undergo two quasi-reversible one-electron reductions, which occurred at $E_{p,c} = -1.06$ and -1.60 V, respectively. The first reduction corresponds to formation of radical anions, and the second reduction relates to formation of dianions.[17] Two separated reduction peaks peculiar to the pyromellitimide diimide segment indicate a facile electronic communication between the two imide units. Similar result was observed with the BPDA polyimide **MeO-3b** [Fig. 7(b)]; however, the first reduction process ($E_{pc} = -1.24$ V) occurred at a more negative potential than observed for the PMDA

TABLE 3 Redox Potentials and Energy Levels of Polyimides

	Thin films (nm)		Oxidation Potential[a] (V)			Reduction Potential[b] (V)			Bandgap[c] (eV)		Energy Levels[d] (eV)	
Polymer code	λ_{max}	λ_{onset}	E_{onset}	$E_{1/2}^{Ox1}$	$E_{1/2}^{Ox2}$	E_{onset}	$E_{1/2}^{Red1}$	$E_{1/2}^{Red2}$	E_g^{opt}	E_g^{eg}	HOMO	LUMO
3a	299, 320	419	0.89	1.05	1.40[e]	−0.57	−0.65	−1.26	2.96	1.78	5.41	3.63
3b	299, 331	387	0.91	1.07	1.38[e]	−0.81	−1.09	−1.28	3.20	2.24	5.43	3.19
3c	299, 328	385	0.90	1.06	1.36[e]	−1.04	−1.25	–	3.22	2.39	5.42	3.03
3d	299, 330	383	0.93	1.08	1.40[e]	−0.90	−1.10	–	3.23	2.26	5.44	3.18
***t*-Bu-3a**	299, 315	420	0.92	1.01	1.29	−0.55	−0.67	−1.29	2.95	1.76	5.37	3.61
***t*-Bu-3b**	299, 336	393	0.90	1.02	1.30	−0.82	−1.10	−1.31	3.16	2.20	5.38	3.18
***t*-Bu-3c**	299, 331	393	0.88	1.03	1.31	−1.05	−1.25	–	3.16	2.36	5.39	3.03
***t*-Bu-3d**	299, 348	391	0.88	1.05	1.28	−0.92	−1.11	–	3.17	2.24	5.41	3.17
MeO-3a	313, 360	418	0.74	0.92	1.20	−0.51	−0.80	−1.37	2.98	1.80	5.28	3.48
MeO-3b	312, 345	397	0.75	0.91	1.19	−0.87	−1.14	−1.32	3.08	2.13	5.27	3.14
MeO-3c	313, 347	396	0.75	0.90	1.19	−0.97	−1.31	–	3.10	2.29	5.26	2.97
MeO-3d	312, 330	391	0.78	0.90	1.19	−0.88	−1.16	–	3.12	1.86	5.31	3.12

[a] Versus Ag/AgCl in CH_3CN. $E_{1/2}$ = average potential of the redox couple peaks.

[b] Versus Ag/AgCl in DMF.

[c] Bandgaps calculated from absorption edge of the polymer films: $E_g^{opt} = 1240/\lambda$onset. E_g^{ec}, electrochemical band gap is derived from the difference between HOMO and LUMO values.

[d] The HOMO and LUMO energy levels were calculated from $E_{1/2}^{Ox1}$ and $E_{1/2}^{Red1}$ values of CV curves and were referenced to ferrocene (4.8 eV; $E_{1/2} = 0.44$ V in CH_3CN; $E_{1/2} = 0.52$ V in DMF).

[e] The second oxidation redox couple is irreversible.

polyimide **MeO-3a**. Only one pair of redox waves was observed for the imide reduction of ODPA polyimide **MeO-3c** [Fig. 7(c)] and 6FDA polyimide **MeO-3d** [Fig. 7(d)] during the negative CV scanning, indicating that the conjugation across the imide is interrupted by the ether and hexafluoroisopropylidene bridges. If two phthalimide groups were connected by a nonconjugated bridge, the generated radicals in each part could not be coupled to form a more stable quinoid dianion. With ether or hexafluoroisopropylidene as the connector, reduction of each phthalimide group occurred at nearly the same position. All the 6FDA polyimides showed the lower reduction potentials than that of the ODPA polyimides due to the electron-withdrawing nature of the hexafluoroisopropylidene linker.

The energy levels of the highest occupied molecular orbital (HOMO) and lowest unoccupied molecular orbital (LUMO) of the corresponding polymers were estimated from the $E_{1/2}^{Ox1}$ and $E_{1/2}^{Red1}$ values. Assuming that the HOMO energy level for the ferrocene/ferrocenium (Fc/Fc^+) standard is 4.80 eV with respect to the zero vacuum level, the HOMO and LUMO values for all polyimides were calculated to be in the range of 5.26–5.44 eV and 2.97–3.63 eV, respectively.

Spectroelectrochemical and Electrochromic Properties

The electro-optical properties of the polymer films were investigated using the changes in electronic absorption spectra at various applied voltages. The results of the cast films of representative polyimides **3d**, ***t*-Bu-3d** and **MeO-3d** upon electro-oxidation (p-doping) are presented in Figure 8 as a series of UV-vis-NIR absorption profiles correlated to electrode potentials. In the neutral form, polyimide **3d** exhibited strong absorptions at 296 and 330 nm, characteristic of the π-π^* transitions of the carbazole and triphenylamine units, but it was almost transparent in the visible and NIR regions. Upon oxidation (increasing applied voltage from 0.0 to 1.1 V), the intensity of the absorption band at 296–330 nm gradually decreased while a new peak at 412 nm and a broad band from 800 nm extended to 1100 nm in the NIR region gradually increased in intensity. These absorptions can be attributed to the formation of the aminyl radical cations. Because of the intervalence charge transfer (IVCT) interactions with the adjacent amino groups, the aminyl radical cations usually show absorption in the NIR region. The IVCT phenomenon of the family of triarylamines has also been reported in the literature.[18] As the anodic potential was further increased to 1.5 V, the absorption bands of the cation radical decreased gradually with a new strong absorption band centered at around 768 nm. The decrease of NIR absorption intensity can be attributable to the further oxidation of monocation radical species to the formation of dication in CzTPA segments. The other two polyimides ***t*-Bu-3d** and **MeO-3d** showed a similar spectral change to that of **3d**. The observed UV–vis-NIR spectral changes in the polyimide films of ***t*-Bu-3d** and **MeO-3d** at various potentials are fully reversible and are associated with strong color changes. From the photos shown in Table 4, these polyimides show a color change from a nearly colorless neutral state to a pale green semi-oxidized state and a blue fully oxidized state during p-doping. However, the spectra and color changes of the film of polyimide **3d** are irreversible during the electro-oxidation process. After the first spectroelectrochemical series of **3d** was recorded from 0.0 to +1.5 V and then back to 0.0 V, we reapplied the electrode voltage and recorded it absorption profile. As shown in Figure 8(b), we observed

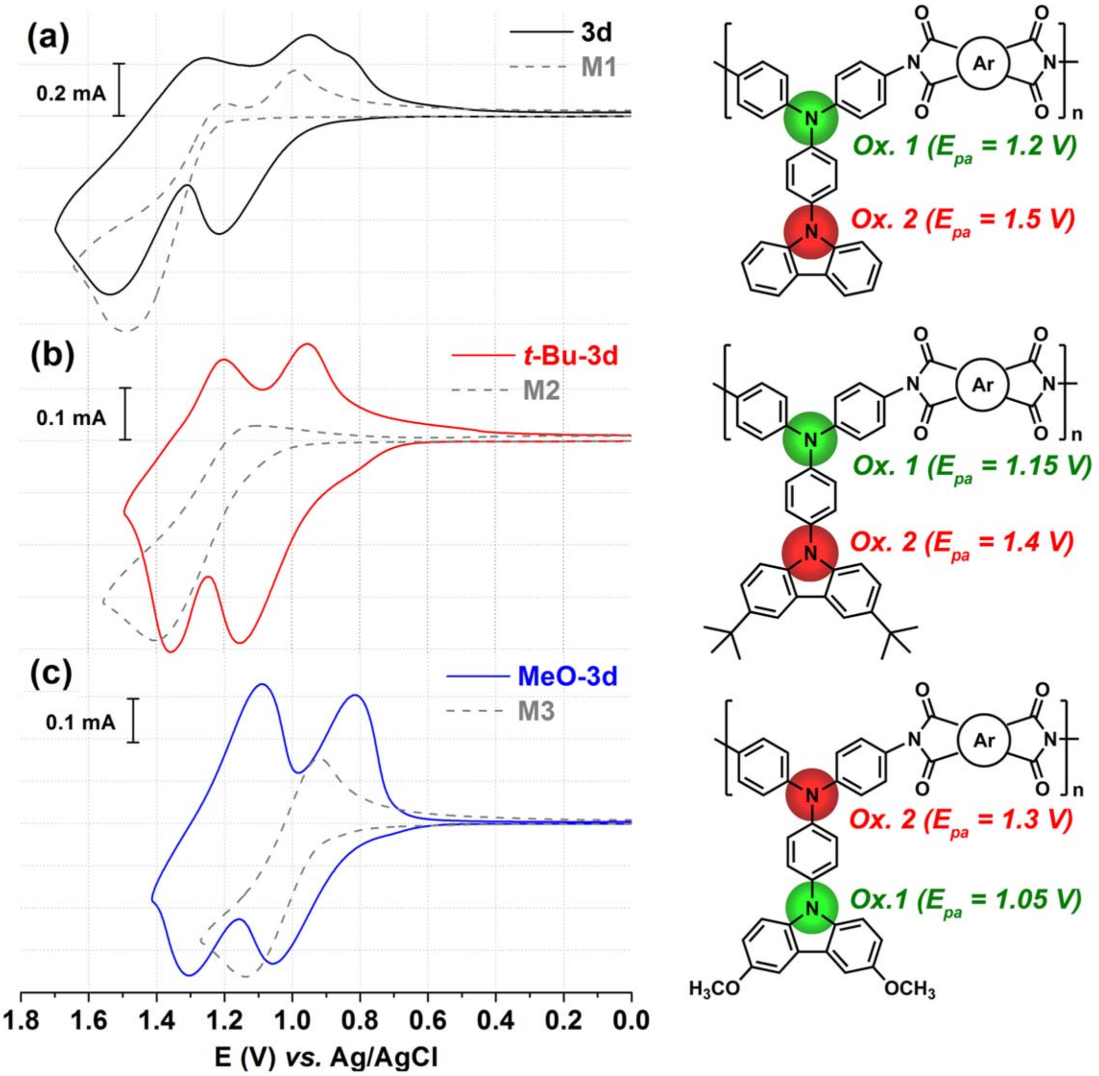

FIGURE 6 First anodic CV scans of the cast films of polyimides **3d**, ***t*-Bu-3d**, and **MeO-3d** on the ITO-coated glass substrates and model compounds **M1-M3** (~ 1 × 10^{-3} M) in 0.1 M Bu_4NClO_4/CH_3CN solution at a scan rate of 50 mV/s. The right shows the possible order of the oxidation reactions in the CzTPA segments of these polyimides. [Color figure can be viewed in the online issue, which is available at wileyonlinelibrary.com.]

a new absorption profile of **3d** at +1.6 V, with the longer-wavelength absorption maximum shifting to 756 nm. The fully oxidized film became pale orange with a significantly decreased optical contrast. The film could not be switched to blue coloring oxidized state anymore. Apparently, a new product was formed via the intermolecular oxidative coupling of the carbazole units during the first potential scan. On the contrary, the spectral changes in the second spectroelectrochemical series of polyimides ***t*-Bu-3d** and **MeO-3d** are almost the same with those observed in the first series. The optical contrast measured as △*T*% of ***t*-Bu-3d** and **MeO-3d** between neutral colorless and oxidized blue states was found to be 88% at 771 nm and 86% at 817 nm, respectively. Thus, the introduction of *tert*-butyl or methoxy group at the electrochemically active C-3 and C-6 sites of the carbazole unit greatly enhances the redox and electrochromic stability of these polyimides.

The polyimide films also exhibited a strong coloration change upon electrochemical reduction. Figure 9 shows the spectral changes of the cast films of polyimides **MeO-3a** and **MeO-3b** upon electro-reduction (n-doping). The radical anion of polyimide **MeO-3a**, which appears at potential −1.05 V, exhibits a strong band at 312 nm and an increased absorption between 654 and 723 nm. As shown Table 4, the radical anion form of polyimide **MeO-3a** is light green in color (L^*: 67; a^*:−6; b^*: 4). Further reduction at potentials negative to −1.60 V results in the two-electron reduced (dianion) state with a new strong absorption at 564 nm, and the film turns to a pink color (L^*: 53; a^*: 25; b^*: −17) during the second-step reduction. The spectral changes associated with the electroreduction reactions of the pyromellitimide unit are very similar to that of standard PMDA-ODA polyimide (ODA: 4,4′-oxydianiline).[17] This result reaffirms that the diamine residue has very little direct influence on the

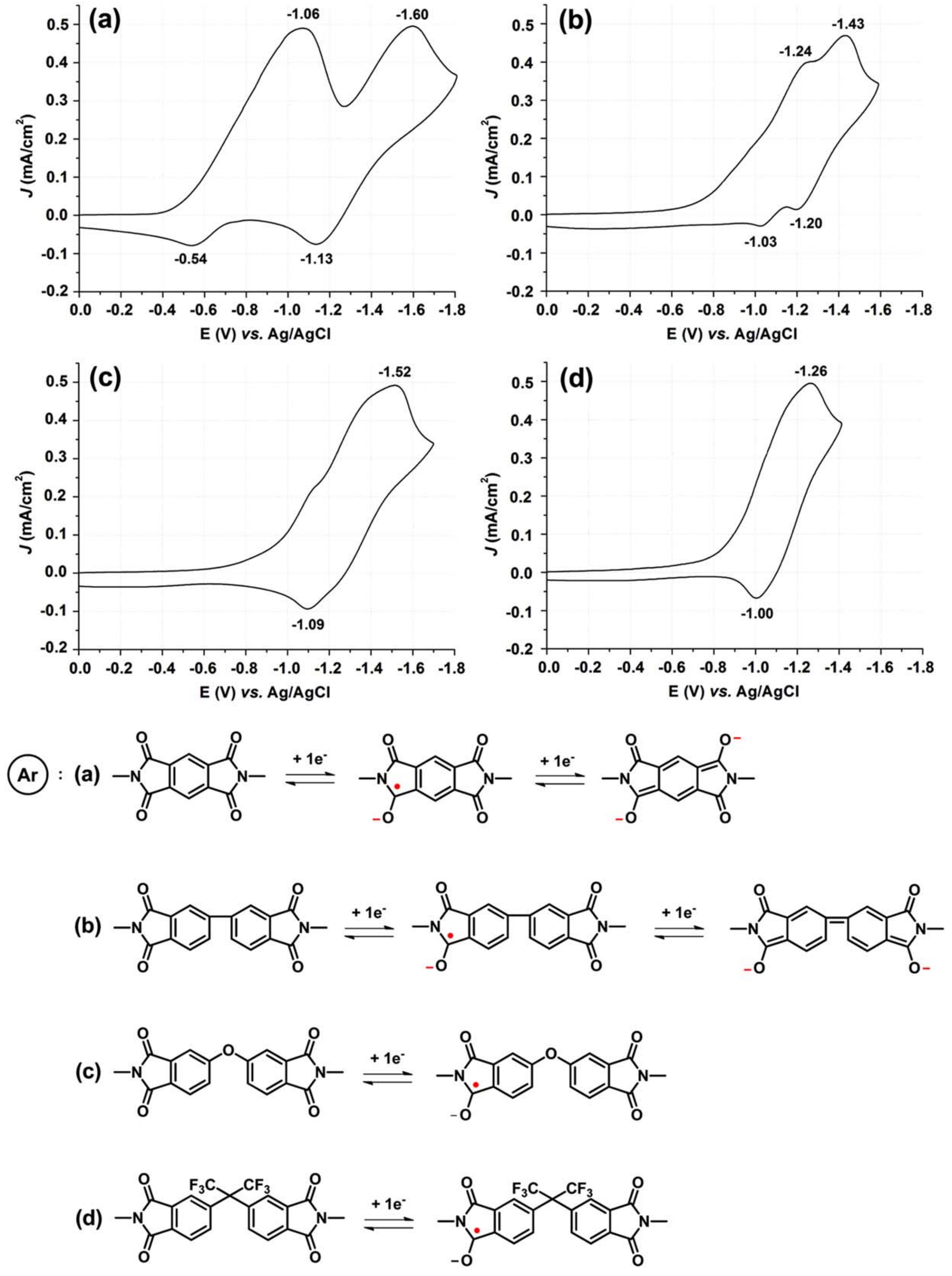

FIGURE 7 Cathodic CV diagrams of the cast films of polyimides (a) **MeO-3a**, (b) **MeO-3b**, (c) **MeO-3c**, and (d) **MeO-3d** on the ITO-coated glass substrate in 0.1 M Bu_4NClO_4/DMF at a scan rate of 100 mV/s. [Color figure can be viewed in the online issue, which is available at wileyonlinelibrary.com.]

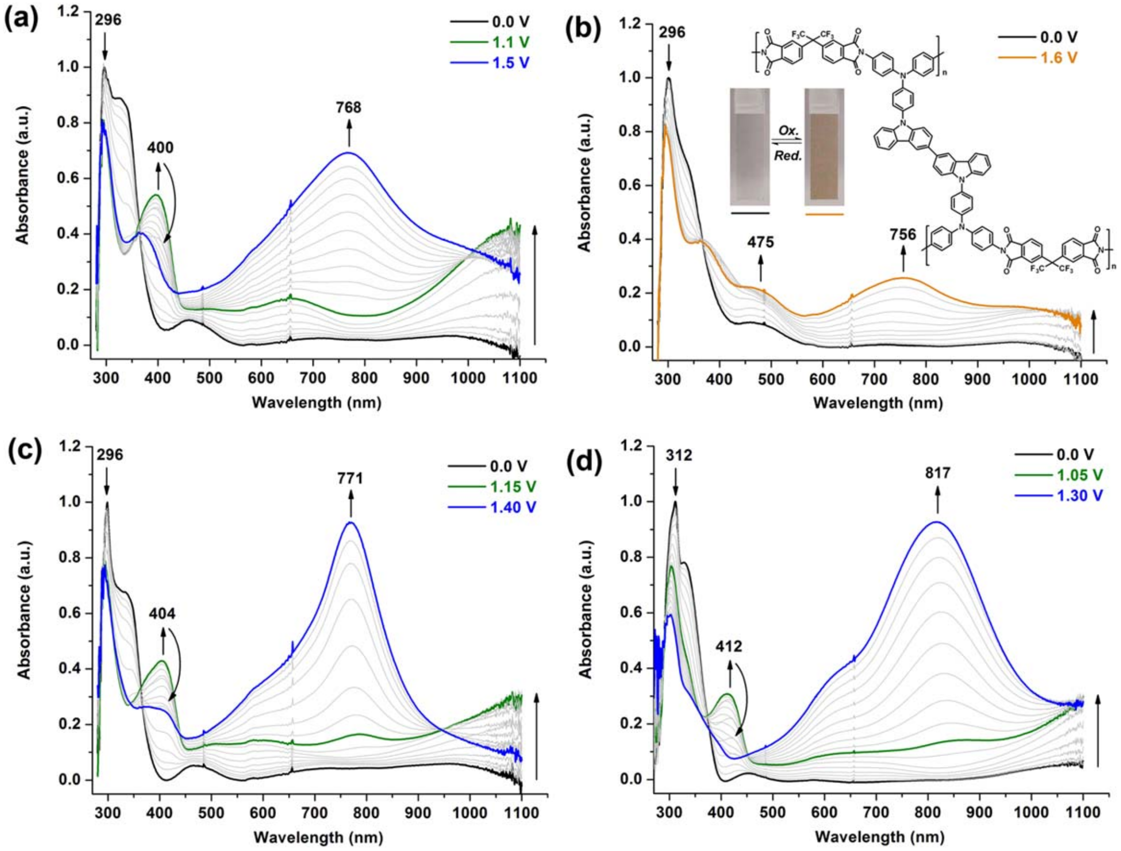

FIGURE 8 Spectral changes of the cast films of polyimides (a) **3d**, (c) ***t*-Bu-3d**, and (d) **MeO-3d** on the ITO-coated glass substrate in 0.1 M Bu_4NClO_4/CH_3CN at various potentials; (b): spectral changes of the **3d** film in the second potential scan. [Color figure can be viewed in the online issue, which is available at wileyonlinelibrary.com.]

TABLE 4 Images and Color Coordinates of Electrochromic Polyimide Films at Indicated Applied Voltages

Polymers	**3d**			***t*-Bu-3d**			**MeO-3d**		
E (V)	0.0	1.2	1.5	0.0	1.15	1.4	0.0	1.05	1.3
Colors									
*L**	95	55	49	96	57	49	96	53	37
*a**	−1	2	−1	−2	3	−6	1	−2	−5
*b**	2	0	−4	1	−3	−15	3	6	−22

Polymers	**MeO-3a**			**MeO-3b**		
E (V)	0.0	−1.05	−1.60	0.0	−1.25	−1.45
Colors						
*L**	96	67	53	96	60	53
*a**	−22	−6	25	1	3	−2
*b**	3	4	−17	3	20	6

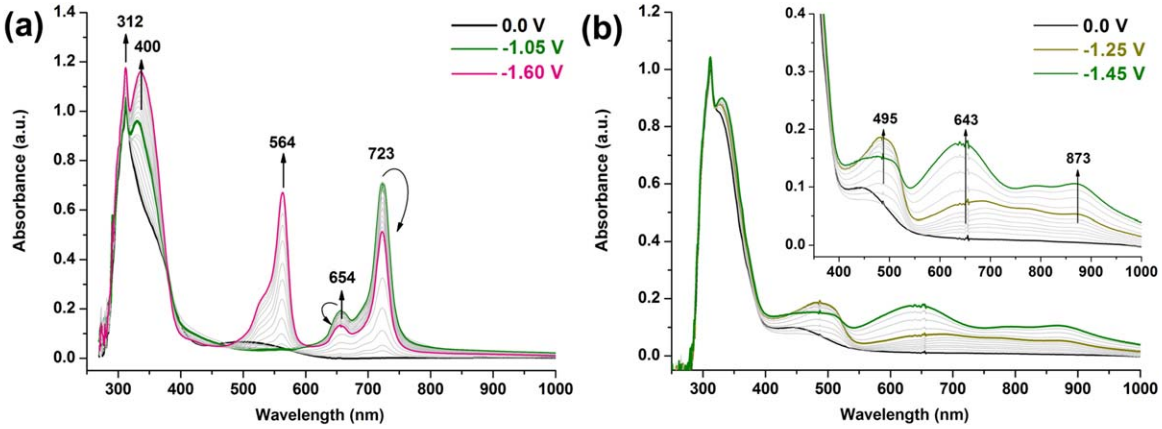

FIGURE 9 Spectral changes of the cast films of polyimides (a) **MeO-3a** and (b) **MeO-3b** on an ITO-glass substrate in 0.1 M Bu_4NClO_4/DMF at various applied potentials. [Color figure can be viewed in the online issue, which is available at wileyonlinelibrary.com.]

reduction of the diimide moiety as reported in literature.[17] The radical anion of polyimide **MeO-3b** formed at −1.25 V reveals a new absorption band in the visible region at about 495 nm, and the film appears as yellow-orange in color (L^*: 60; a^*: 3; b^*: −20). As the film was further charged with electrons at −1.45 V, the absorption intensity at 495 nm decreased slightly, and two new bands emerged at about 643 and 873 nm, and the film turned to a green-blue color (L^*: 53; a^*: −2; b^*: −6) during the second-step reduction.

CONCLUSIONS

Three series of aromatic polyimides with CzTPA units have been successfully prepared from the polycondensation reactions of CzTPA-based diamine monomers **1**, ***t*-Bu-1**, and **MeO-1**, respectively, with commercially available tetracarboxylic dianhydrides. Incorporating bulky *tert*-butyl or electron-donating methoxy substituents at the electrochemically active C-3 and C-6 sites of the carbazole unit prevents the coupling reactions of carbazoles and leads to a greatly enhanced redox and electrochromic stability of the resulting polyimides upon electro-oxidation. In addition to good thermal stability and film-forming ability, the ***t*-Bu-** and **MeO-**series polyimides also revealed valuable electrochromic characteristics in both visible and NIR regions. Thus, these polyimides may find optoelectronic applications as new hole-transporting and electrochromic materials.

REFERENCES AND NOTES

1 (a) Polyimides; D. Wilson, H. D. Stenzenberger, P. M. Hergenrother, Eds.; Blackie: Glasgow and London, **1990**; (b) C. E. Sroog, *Prog. Polym. Sci.* **1991**, *16*, 561–694; (c) *Polyimides: Fundamentals and Applications*; M. K. Ghosh, K. L. Mittal, Eds.; Marcel Dekker: New York, **1996**.

2 (a) S. J. Huang, A. E. Hoyt, *TRIP* **1995**, *3*, 262–271; (b) J. de Abajo, J. G. de la Campa, *Adv. Polym. Sci.* **1999**, *140*, 23–59; (c) M. Ding, *Prog. Polym. Sci.* **2007**, *32*, 623–668; (d) M. G. Dhara, S. Banerjee, *Prog. Polym. Sci.* **2010**, *35*, 1022–1077; (e) D.-J. Liaw, K.-L. Wang, Y.-C. Huang, K.-R. Lee, J.-Y. Lai, C.-S. Ha, *Prog. Polym. Sci.* **2012**, *37*, 907–974.

3 (a) S.-H. Hsiao, K.-H. Lin, *J. Polym. Sci. Part A: Polym. Chem.* **2005**, *43*, 331–341; (b) S. M. Kwak, J. H. Yeon, T. H. Yoon, *J. Polym. Sci. Part A: Polym. Chem.* **2006**, *44*, 2567–2578; (c) Y.-T. Chern, J.-Y. Tsai, J.-J. Wang, *J. Polym. Sci. Part A: Polym. Chem.* **2009**, *47*, 2443–2452; (d) C. W. Chung, C. H. Lin, P. W. Cheng, H. J. Hwang, S. Dai, *J. Polym. Sci. Part A: Polym. Chem.* **2009**, *47*, 2486–2499; (e) S. J. Zhang, Y. F. Li, T. Ma, J. J. Zhao, X. Y. Xu, F. C. Yang, X. Y. Xiang, *Polym. Chem.* **2010**, *1*, 485–493; (f) Y. Liu, Y. Xing, Y. H. Zhang, S. W. Guan, H. B. Zhang, Y. Wang, Y. P. Wang, Z. H. Jiang, *J. Polym. Sci. Part A: Polym. Chem.* **2010**, *48*, 3281–3289; (g) M. Calle, A. E. Lozano, J. G. de la Campa, J. de Abajo, *Macromolecules* **2010**, *43*, 2268–2275; (h) C. H. Lin, S. L. Chang, P. W. Cheng, *J. Polym. Sci. Part A: Polym. Chem.* **2011**, *49*, 1331–1340; (i) H. B. Wei, X. L. Pei, X. Z. Fang, *J. Polym. Sci. Part A: Polym. Chem.* **2011**, *49*, 2484–2494; (j) S.-H. Hsiao, H.-M. Wang, W.-J. Chen, T.-M. Lee, C.-M. Leu, *J. Polym. Sci. Part A: Polym. Chem.* **2011**, *49*, 3109–3120; (k) Y. J. Hou, G. F. Chen, X. L. Pei, X. Z. Fang, *J. Polym. Res.* **2012**, *19*, 9955.

4 (a) Y. Shirota, *J. Mater. Chem.* **2000**, *10*, 1–25; (b) M. Thelakkat, *Macromol. Mater. Eng.* **2002**, *287*, 442–461; (c) Y. Shirota, *J. Mater. Chem.* **2005**, *15*, 75–93; (d) Y. Shirota, H. Kageyama, *Chem. Rev.* **2007**, *107*, 953–1010.

5 (a) M.-H. Tsai, T.-H. Ke, H.-W. Lin, C.-C. Wu, S.-F. Chiu, F.-C. Fang, Y.-L. Liao, F.-T. Wong, Y.-H. Chen, C.-I Wu, *ACS Appl. Mater. Interfaces* **2009**, *1*, 567–574; (b) Y.-T. Tao, Q. Wang, C.-L. Yang, C. Zhong, K. Zhang, J.-G. Qin, D.-G. Ma, *Adv. Funct. Mater.* **2010**, *20*, 304–311; (c) W. Jiang, L. Duan, J. Qiao, G.F. Dong, D.-Q. Zhang, L.-D. Wang, Y. Qiu, *J. Mater. Chem.* **2011**, *21*, 4918–4926; (d) L.-X. Xiao, Z.-J. Chen, B. Qu, J.-X. Luo, S. Kong, Q.-H. Gong, J. Kido, *Adv. Mater.* **2011**, *23*, 926–952; (e) Y.-T. Tao, C.-L. Yang, J.-G. Qin, *Chem. Soc. Rev.* **2011**, *40*, 2943–2970.

6 (a) F. Liang, T. Kurata, H. Nishide, J. Kido, *J. Polym. Sci. Part A: Polym. Chem.* **2005**, *43*, 5765–5773; (b) Y.-H. Kim, Q. Zhao, S.-K. Kwon, *J. Polym. Sci. Part A: Polym. Chem.* **2006**, *44*, 172–182; (c) Q. Zhao, Y.-H. Kim, T. T. Mai Dang, D.-C. Shin, H. You, S.-K. Kwon, *J. Polym. Sci. Part A: Polym. Chem.* **2007**, *45*, 341–347; (d) J. H. Park, J. O. Huh, Y. Do, M. H. Lee, *J. Polym. Sci. Part A: Polym. Chem.* **2008**, *46*, 5816–5825; (e) B.-Y. Hsieh, Y. Chen, *J. Polym. Sci. Part A: Polym. Chem.* **2009**, *47*, 1553–1566; (f) H. Li, L. Wang, B. Zhao, P. Shen, S. Tan, *J. Polym. Sci. Part A: Polym. Chem.* **2009**, *47*, 3296–3308; (g) M. W. Thesen, B. Hofer, M. Debeaux, S. Janietz,

A. Wedel, A. Kohler, H.-H. Johannes, H. Krueger, *J. Polym. Sci. Part A: Polym. Chem.* **2010**, *48*, 3417–3430.

7 (a) S. Beaupre, J. Dumas, M. Leclerc, *Chem. Mater.* **2006**, *18*, 4011–4018; (b) L. Otero, L. Sereno, F. Fungo, Y.-L. Liao, C.-Y. Lin, K.-T. Wong, *Chem. Mater.* **2006**, *18*, 3495–3502; (c) J. Natera, L. Otero, L. Sereno, F. Fungo, N.-S. Wang, Y.-M. Tsai, T.-Y. Hwu, K.-T. Wong, *Macromolecules* **2007**, *40*, 4456–4463; (d) J. Natera, L. Otero, F. D'Eramo, L. Sereno, F. Fungo, N.-S. Wang, Y.-M. Tsai, K.-T. Wong, *Macromolecules* **2009**, *42*, 626–635.

8 (a) S.-H. Cheng, S.-H. Hsiao, T.-H. Su, G.-S. Liou, *Macromolecules* **2005**, *38*, 307–316; (b) S.-H. Hsiao, Y.-M. Chang, H.-W. Chen, G.-S. Liou, *J. Polym. Sci. Part A: Polym. Chem*. **2006**, *44*, 4579–4592; (c) H.-M. Wang, S.-H. Hsiao, *Polymer* **2009**, *50*, 1692–1699; (d) S.-H. Hsiao, G.-S. Liou, Y.-C. Kung, H.-Y. Pan, C.-H. Kuo, *Eur. Polym. J.* **2009**, *45*, 2234–2248; (e) Y.-C. Kung, S.-H. Hsiao, *J. Mater. Chem.* **2011**, *21*, 1746–1754; (f) Y.-C. Kung, W.-F. Lee, S.-H. Hsiao, G.-S. Liou, *J. Polym. Sci. Part A: Polym. Chem*. **2011**, *49*, 2210–2221.

9 (a) C.-W. Chang, G.-S. Liou, S.-H. Hsiao, *J. Mater. Chem.* **2007**, *17*, 1007–1015; (b) S.-H. Hsiao, G.-S. Liou, Y.-C. Kung, H.-J. Yen, *Macromolecules* **2008**, *41*, 2800–2808; (c) Y.-C. Kung, G.-S. Liou, S.-H. Hsiao, *J. Polym. Sci. Part A: Polym. Chem*. **2009**, *47*, 1740–1755; (d) S.-H. Hsiao, G.-S. Liou, H.-M. Wang, *J. Polym. Sci. Part A: Polym. Chem.* **2009**, *47*, 2330–2343; (e) S.-H. Hsiao, G.-S. Liou, Y.-C. Kung, Y.-M. Chang, *J. Polym. Sci. Part A: Polym. Chem*. **2010**, *48*, 2798–2809; (g) H.-M. Wang, S.-H. Hsiao, *J. Polym. Sci. Part A: Polym. Chem*. **2011**, *49*, 337–351.

10 (a) G.-S. Liou, S.-H. Hsiao, H.-W. Chen, *J. Mater. Chem.* **2006**, *16*, 1831–1842; (b) G.-S. Liou, H.-W. Chen, H.-J. Yen, *J. Polym. Sci. Part A: Polym. Chem.* **2006**, *44*, 4108–4121; (c) G.-S. Liou, S.-H. Hsiao, N.-K. Huang, Y.-L. Yang, *Macromolecules* **2006**, *39*, 5337–5346.

11 (a) J. A. Ambrose, R. F. Nelson, *J. Electrochem. Soc. Electrochem. Sci.* **1968**, *115*, 1159–1164; (b) J. A. Ambrose, L. L. Carpenter, R. F. Nelson, *J. Electrochem. Soc. Electrochem. Sci. Technol.* **1975**, *122*, 876–894.

12 (a) M.-H. Tsai, H.-W. Lin, H.-C. Su, T.-H. Ke, C.-C. Wu, F.-C. Fang, Y.-L. Liao, K.-T. Wong, C.-I Wu, *Adv. Mater.* **2006**, *18*, 1216–1220; (b) Y. T. Tao, S. L. Gong, Q. Wang, C. Zhang, C. L. Yang, J. G. Gin, D. G. Ma, *Phys. Chem. Chem. Phys*. **2010**, *12*, 2438–2442.

13 S.-H. Hsiao, H.-M. Wang, S.-H. Liao, *Polym. Chem.*, in press, DOI:10.1039/C3PY01239E.

14 H.-M. Wang, S.-H. Hsiao, *J. Mater. Chem. C*, **2014**, *2*, 1553–1564. DOI: 10.1039/C3TC32005G.

15 H.-M. Wang, S.-H. Hsiao, *J. Polym. Sci. Part A: Polym. Chem.* **2014**, *52*, 272–286.

16 S.-K. Chiu, Y.-C. Chung, G.-S. Liou, Y. O. Su, *J. Chin. Chem. Soc.* **2012**, *59*, 331–337.

17 (a) S. Mazur, P. S. Lugg, C. Yarnitzky, *J. Electrochem. Soc. Electrochem. Sci. Technol.* **1987**, *134*, 346–353; (b) A. Viehbeck, M. J. Goldberg, C. A. Kovac, *J. Electrochem. Soc.* **1990**, *137*, 1460–1466.

18 (a) C. Lambert, G. Noll, *J. Am. Chem. Soc.* **1999**, *121*, 8434–8442; (b) A. V. Azeghalmi, M. Erdmann, V. Kriegisch, G. Noll, R. Stahl, C. Lambert, D. Leusser, D. Stalke, M. Zabel, J. Popp, *J. Am. Chem. Soc*. **2004**, *126*, 7834–7845.